Available online at www.sciencedirect.com
ScienceDirect
Journal of Power Sources 161 (2006) 294–300
JOURNAL OF POWER SOURCES
www.elsevier.com/locate/jpowsour

Analysis of coupled electron and mass transport in the gas diffusion layer of a PEM fuel cell

P.C. Sui, N. Djilali *

Institute for Integrated Energy Systems, University of Victoria, PO Box 3055 STN CSC, Victoria, BC V8W 3P6, Canada

Received 15 January 2006; received in revised form 23 March 2006; accepted 28 March 2006
Available online 24 May 2006

Abstract

A numerical investigation of the coupled electrical conduction and mass diffusion in the cathodic GDL of a PEMFC is performed using 2D simulations. The current density on the GDL/catalyst layer interface, which constitutes one of the boundary conditions for the GDL domain and reflects the activation overpotential in the catalyst layer and the ohmic loss in the membrane, is solved iteratively using a novel numerical algorithm. A parametric study is performed to investigate the effects on current density distribution of various operating conditions such as oxygen concentration and membrane resistance, and of design factors such as GDL geometry, anisotropic transport properties, and deformation under the land area due to compression. The results show that the current density distribution under the land area can be dominated by either electron transport or mass transport, depending on the operating regime. The analysis of the in-plane current density gradients shows the contributions due to electrical conduction, oxygen diffusion and membrane resistance in an explicit form. The analysis also provides guidance for the scaling of the coupled transport problem.

Keywords: Fuel cell; Gas diffusion layer; Proton exchange membrane; Membrane electrode assembly; Conduction; Diffusive transport

1. Introduction

In most planar proton exchange membrane fuel cell (PEMFC) designs the membrane electrode assembly (MEA) is sandwiched between bipolar plates. The interface between the bipolar plates and the MEA, or 'land', is where electric current flows in/out of the MEA. The impact of the land area on fuel cell operation has been investigated numerically by Kulikovsky et al. [1], Meng and Wang [2], Nguyen et al. [3], Ziegler et al. [4] and recently Sun et al. [5] amongst others. In these 2D or 3D computational simulations, higher current density distributions under the land area were reported for typical operating conditions and for a conventional channel/land geometry. The shift in current distribution patterns, and in particular of the maximum current density location from the land to the channel area under some operating conditions highlights the trade-offs between electrical and diffusive transport. The non-uniform current density distribution under the land associated with a specific land/channel geometry is expected to have a significant impact on the transport phenomena in the lateral direction within the MEA. Indeed the gradients in the lateral direction may be the largest in the entire fuel cell. From a design standpoint, understanding the effects of the land is therefore crucial.

Many of the contributions made in the last few years to computational analysis of PEM fuel cells have been discussed in a thorough review [6] and notable earlier work includes Berning et al. [7], Mazumder and Cole [8], Lee et al. [9], Meng and Wang [2], and Nguyen et al. [3]. Some more recent representative contributions include parallelized three-dimensional CFD modelling [10,11,12] parametric computational studies and validation [13]; developments addressing the important aspects of two-phase transport [14] and catalyst layer modelling [15]. Most of the aforementioned works involved numerical solutions of a full set of complex and coupled transport equations, and typically include the complete fuel cell geometry. While allowing high fidelity, such computations are intensive and often impractical for design or optimization purposes. The aim of this work is to develop a simplified model that accounts for the salient and dominant processes associated with coupled electron and mass transport inside the GDL. A 2D configuration is thus considered

* Corresponding author. Tel.: +1 250 721 6034; fax: +1 250 721 6323.
E-mail address: ndjilali@uvic.ca (N. Djilali).

0378-7753/$ – see front matter © 2006 Elsevier B.V. All rights reserved.
doi:10.1016/j.jpowsour.2006.03.079

Nomenclature

D	mass diffusivity ($m^2\ s^{-1}$)
f	F/R_uT
F	Faraday constant, 96487 C
i	current density ($A\ m^{-2}$)
i_0	cathode exchange current density ($A\ m^{-2}$)
M_{O_2}	oxygen molecular weight ($kg\ mol^{-1}$)
P	pressure (Pa)
R_{mem}	membrane resistance (Ω)
R_u	universal gas constant, $8.314\ J\ mol^{-1}\ K^{-1}$
T	temperature (K)
x	X-coordinate (in-plane)
x_{O_2}	oxygen mole fraction
y	Y-coordinate (through-plane)

Greek letters

α_c	cathode transfer coefficient
η	activation overpotential (V)
ρ	mass density of mixture ($kg\ m^{-3}$)
σ	electrical conductivity ($\Omega^{-1}\ m^{-1}$)
ϕ	electrical potential (V)

Subscripts

BC	on the GDL/catalyst layer interface
ref	reference value
xx	in-plane direction of the GDL
yy	through-plane direction of the GDL

Superscripts

N	current iteration step
*	on the anode bipolar plate

for the GDL taking into account the influences of the catalyst layer and the membrane on one of the GDL boundaries. The main objective is to develop a model that adequately describes the coupling and that is suitable for design and optimization purposes, where rapid turnaround is required.

2. Mathematical formulation and numerical method

We consider the transport processes in the half GDL domain, cf. Fig. 1, which is bounded by the GDL/catalyst layer interface at the bottom, and by a half-land and a half-channel at the top. The governing equations that describe the transport of electron and oxygen are, respectively

$$\sigma_{xx}\frac{\partial^2\phi}{\partial x^2} + \sigma_{yy}\frac{\partial^2\phi}{\partial y^2} = 0 \tag{1}$$

$$D_{xx}\frac{\partial^2 x_{O_2}}{\partial x^2} + D_{yy}\frac{\partial^2 x_{O_2}}{\partial y^2} = 0 \tag{2}$$

where subscript xx denotes the value in the in-plane direction and subscript yy denotes the value in the through-plane. The boundary conditions for the governing equations are: (i) symmetry condition for the side boundaries of the domain, (ii) prescribed

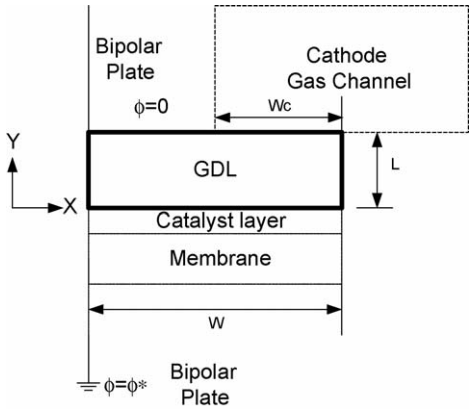

Fig. 1. Computational domain of the 2D GDL problem.

potential and zero oxygen flux on the land, (iii) prescribed oxygen mole fraction and zero current on the gas channel boundary, and (iv) prescribed current and oxygen flux on the GDL/catalyst layer interface:

$$\frac{\partial\phi}{\partial y} = \frac{i}{\sigma_{yy}} \tag{3}$$

$$\frac{\partial x_{O_2}}{\partial y} = \frac{M_{O_2}}{\rho D}\frac{i}{4F} \tag{4}$$

Boundary condition (iv) requires information of local current density distribution that satisfies

$$\phi^* = \phi_{BC} + \eta + iR \tag{5}$$

where ϕ^* represents the cell potential at the *anode* side of the bipolar plate, which is the sum of the ohmic loss in the GDL, activation overpotential loss in the cathode catalyst layer, and ohmic loss across the membrane. All other losses on the anode side of the MEA are assumed negligible. Eq. (5), hereafter called 'potential balance equation', is a boundary condition required to close the model. The purpose of introducing such a potential is that one can conveniently include the effects of the catalyst layer and the membrane into the solution procedure even though only transport in the GDL is directly solved. A Butler–Volmer type of expression is adopted for the activation overpotential:

$$\eta = \frac{1}{\alpha_c f}\ln\left[\frac{i}{i_0}\left(\frac{P_{ref}x_{O_2}^{ref}}{Px_{O_2}}\right)\right] \tag{6}$$

It is noted that the two transport processes considered in the problem are only coupled at the GDL/catalyst layer interface.

The potential loss ϕ^* is not known a priori, and is assumed to be uniform on the anode bipolar plate. An iterative method for calculating this potential loss using an updated current density profile based on local oxygen concentration is developed in this study. For each iteration, we compute a new $\bar{\phi}^*$ based on the results from previous iteration:

$$\bar{\phi}^* = \frac{\sum\frac{\eta^N}{R} + \sum\frac{\phi_{BC}^N}{R} + \sum i^N}{\sum\frac{1}{R}} \tag{7}$$

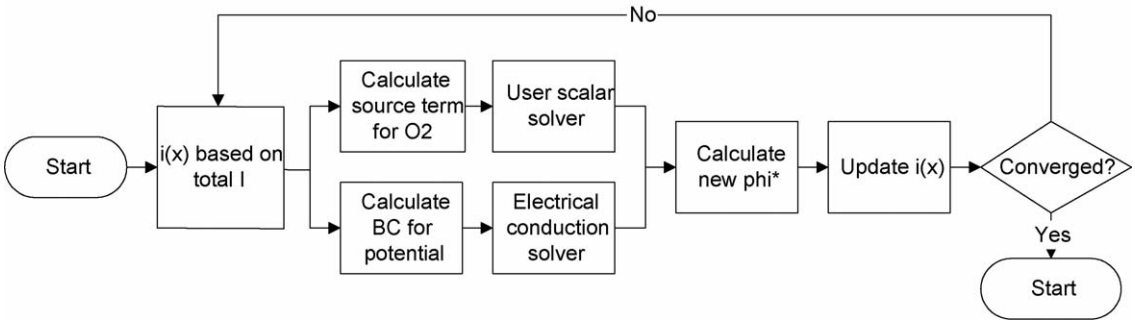

Fig. 2. Flow chart of the solution procedure.

With this $\bar{\phi}^*$ the current density distribution for the next iteration is then calculated by substituting (7) into (5):

$$i^{N+1} = \frac{\bar{\phi}^* - \phi_{\mathrm{BC}}^N - \eta^N}{R} \tag{8}$$

The advantage of evaluating $\bar{\phi}^*$ using (7) is that the total current is conserved *at each iteration*. This can be shown by summing (8) and substituting (7) into the summation:

$$\begin{aligned}\sum i^{N+1} &= \sum \frac{\bar{\phi}^*}{R} - \sum \frac{\phi_{\mathrm{BC}}^N}{R} - \sum \frac{\eta^N}{R} \\ &= \bar{\phi}^* \sum \frac{1}{R} - \sum \frac{\phi_{\mathrm{BC}}^N}{R} - \sum \frac{\eta^N}{R} \\ &= \left(\sum \frac{\eta^N}{R} + \sum \frac{\phi_{\mathrm{BC}}^N}{R} + \sum i^N \right) \\ &\quad - \sum \frac{\phi_{\mathrm{BC}}^N}{R} - \sum \frac{\eta^N}{R} = \sum i^N \end{aligned} \tag{9}$$

A flow chart of the solution procedure is shown in Fig. 2. A commercial CFD software, CFD-ACE+, is used to solve the problem in conjunction with custom written user-defined subroutines.

3. Results and discussion

3.1. Baseline case

Table 1 lists the values of the parameters and dimensions used for the parametric study. The numerical values of α_c and i_0 are obtained by fitting a polarization curve with a comprehensive unit cell model, cf. Mazumder and Cole [8]. The total width of the gas channel and land is 1 mm; with symmetry conditions in the computation, only half of the gas channel and half of the land need to be considered. The effective diffusivity of oxygen should account for the porosity of the GDL and gas concentration, but for simplicity a constant value is used in the calculation. The GDL electrical conductivity used is close to the through-plane conductivity of common carbon paper, which is usually one order of magnitude lower than the in-plane value. A slight variation of the membrane resistance in the in-plane direction is added to reflect the membrane resistance variation due to the conditions in the anode side of the membrane:

$$R_{\mathrm{mem}}(x) = R_{\mathrm{mem}}^0 \left(1 - \frac{2x - w}{w} 0.15 \right) \tag{10}$$

Table 1
Parameter values used for the baseline case

Variable	Symbol	Value	Unit
GDL thickness	L	250	μm
Half-channel width	W_c	0.5	mm
Half-land width	W_l	0.5	mm
Effective oxygen diffusivity	$D_{O_2,\mathrm{eff}}$	1×10^{-5}	$m^2\,s^{-1}$
GDL electrical conductivity	σ	200	$\Omega^{-1}\,m^{-1}$
Membrane resistance	R_{mem}^0	1×10^{-5}	$\Omega\,m^2$
Pressure	P	3	bar
Temperature	T	343	K
Reference oxygen mole fraction	$x_{O_2,\mathrm{ref}}$	0.209	1
Transfer coefficient	α_c	1.15	1
Exchange current density	i_0	1.116	$A\,m^{-2}$
Oxygen concentration exponent	γ	1	1

It should be noted that most of the values listed in Table 1 were extracted from comprehensive 3D simulations of a complete fuel cell and the baseline values are determined from the validation of these simulations with experimental data [16]. In the parametric simulations presented here the average current density is set to 10,000 $A\,m^{-2}$.

3.2. Effects of land/gas channel width ratio

Fig. 3 shows the predicted current density on the GDL/catalyst layer interface for different land:channel ratios ('L:C' in the figure). The baseline case has an L:C ratio of 5:5. For a narrower land, e.g. L:C = 3:7, the higher current density occurs near the land side of the GDL. As the land width is increased, the current density maximum shifts to the gas channel side of the GDL. Since electric current tends to flow in the direction of least resistance, the high current density region on the GDL/catalyst layer indicates that for a narrow land the transport of electrons is dominated by electrical conduction in the GDL, while for the wider land case transport of oxygen becomes dominant. Fig. 4 shows the potential loss of the cell for different L:C ratios. The total potential loss, which consists of the losses in the GDL, catalyst layer and membrane, decreases with land width at first, reaches a minimum near L:C = 5:5 and then increases slightly for wider land. The break-down of the potential losses (note differ-

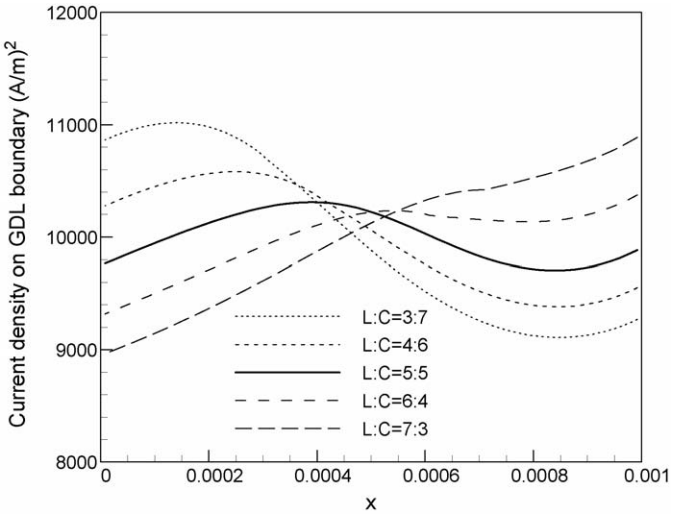

Fig. 3. Current density profiles for different land:channel ratios.

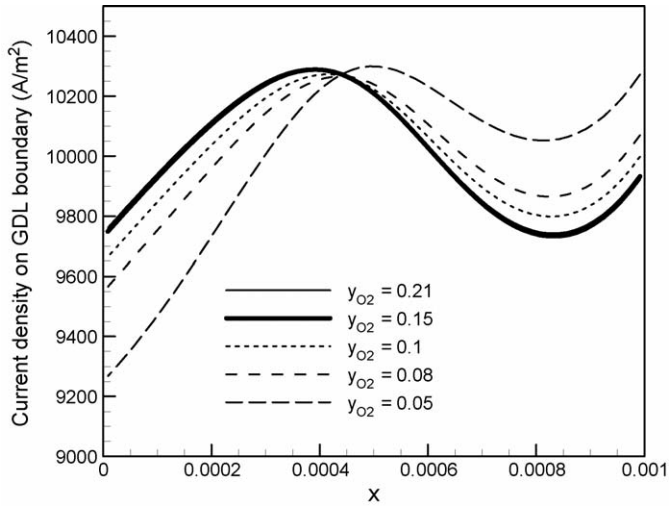

Fig. 5. Current density profiles for different oxygen mole fractions in the gas channel.

ent scales in the figure) shows that the decrease of total potential loss from L:C = 3:7 to 5:5 is mainly due to the decrease of the loss in the GDL. Further increase of the land width does not reduce this loss significantly, rather the loss due to the overpotential in the catalyst layer is increased due to mass diffusion constraints caused by the narrow channel opening.

3.3. Effects of oxygen concentration in the gas channel

Fig. 5 shows the current density predictions for different oxygen mole fraction in the gas channel. As oxygen concentration is decreased, the diffusion of oxygen becomes more dominant in the coupling of the two transport processes in the GDL, and hence the high current density region moves towards the gas channel side of the GDL and the difference of current density becomes larger. Such shifts have been observed earlier by Meng and Wang [2] and Nguyen et al. [3], and more recently by Sun et al. [15]. For a typical fuel cell, low oxygen concentration occurs downstream of the gas channel. Therefore one can expect a similar shift of current density and increase of current density gradient from the channel inlet to the exit in a fuel cell. Fig. 6 shows the total potential loss for the cases shown in Fig. 5. The potential loss increases as oxygen concentration is decreased in the gas channel.

3.4. Effects of electrical conductivity

Fig. 7 shows the current density predictions for different GDL electrical conductivities. Isotropic conduction is assumed for these cases. The effect on the current density distribution is significant for conductivity values lower than the baseline value. For conductivity higher than the baseline value the current density is not sensitive to the conductivity because the loss in the GDL is negligible, cf. Fig. 8, thus the current density distribution is mainly determined by the transport of oxygen.

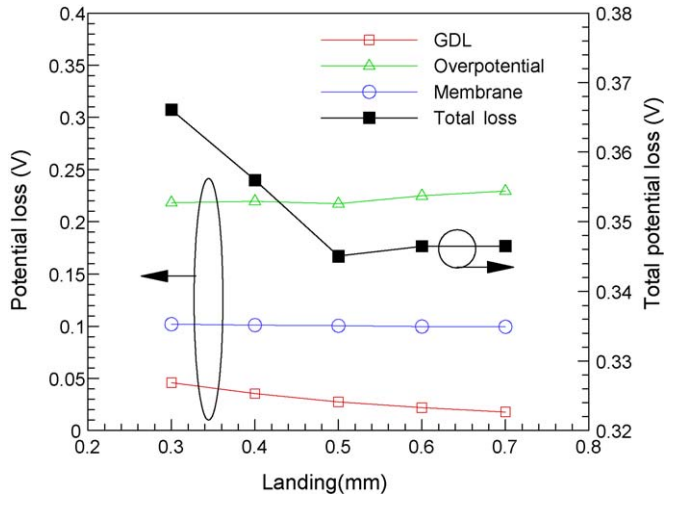

Fig. 4. Potential losses for different land:channel ratios.

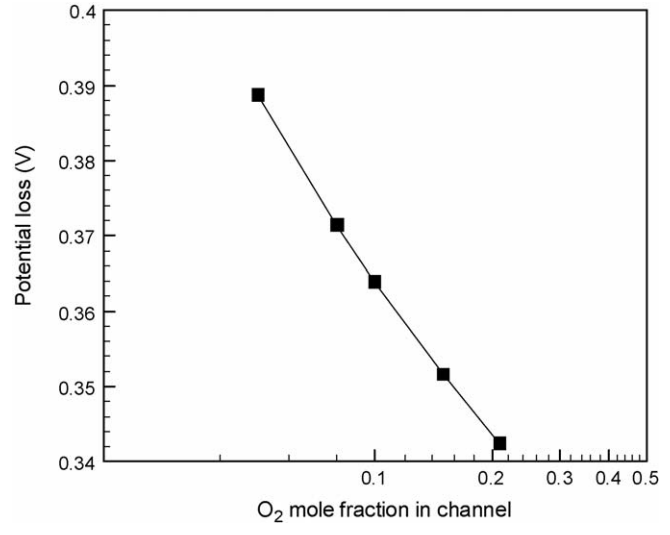

Fig. 6. Potential losses for different oxygen mole fractions in the gas channel.

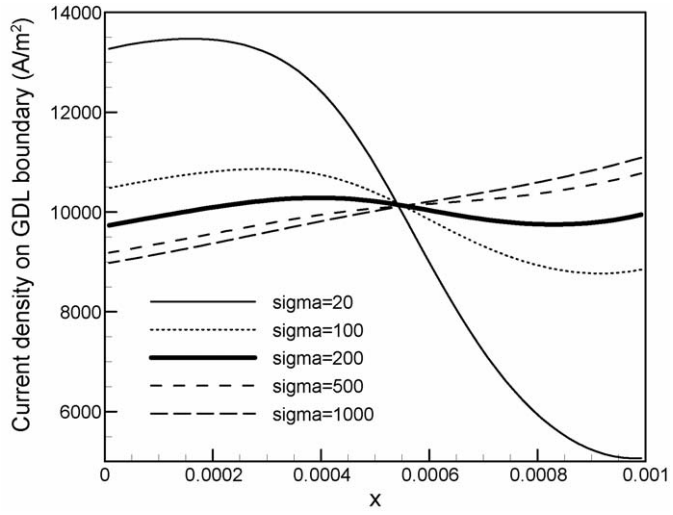

Fig. 7. Current density profiles for different GDL electrical conductivities.

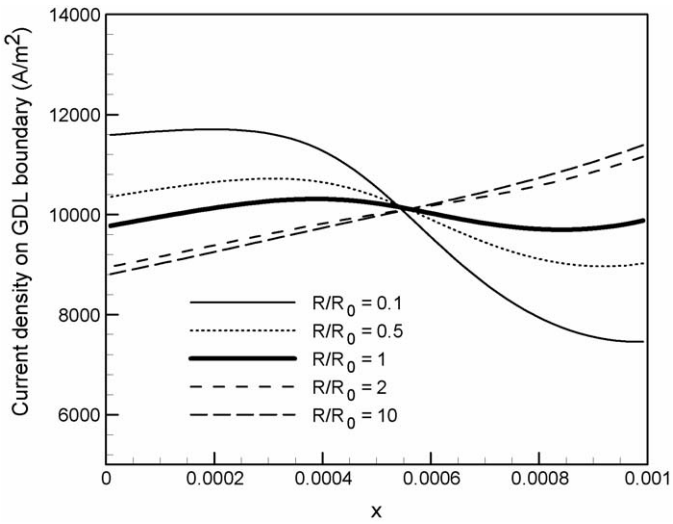

Fig. 9. Current density profiles for different membrane conductivities.

3.5. Effects of membrane resistance

The conduction of protons in the membrane is not directly modeled here, but appears instead as a potential loss term in the potential balance Eq. (5). This implies that the current flow in the membrane is perpendicular to the GDL/catalyst layer interface. In this sense the effect of membrane resistance can be considered as an additional *through-plane* resistance to the electrical conduction in the GDL. Fig. 9 shows the predictions of current density distribution for different membrane resistance values, marked as the ratio with respect to the baseline value R_0 in the figure. One can see that increasing the membrane resistance has a similar effect as decreasing the GDL electrical conductivity, cf. Fig. 7. A similar trend should be expected, though this was not ascertained in the present study, for the contact resistance at the land/GDL interface.

Fig. 10 shows the potential loss increases linearly with membrane resistance values. The implication of the parametric study with membrane resistance is that for a fuel cell that operates under low humidity conditions, such as air-breathing fuel cell or a cell with low anode humidification, the current density distribution in the GDL may be quite different from that in a well-humidified fuel cell.

3.6. Effects of compression

In assembling the bipolar plate and the MEA in a fuel cell, a compression force is always required to ensure proper sealing and to reduce contact resistance between the bipolar plate and the GDL. The GDL is expected to undergo some deformation under such compression as it is the least stiff component in the MEA. The impact of the compression on transport processes in the GDL, in particular the region underneath the land, is likely two-fold: the *through-plane* conductivity of the GDL would increase as new conducting pathways form between the fibres, and the *through-plane* diffusivity of oxygen would be reduced as the porosity is reduced. Based on the observations in

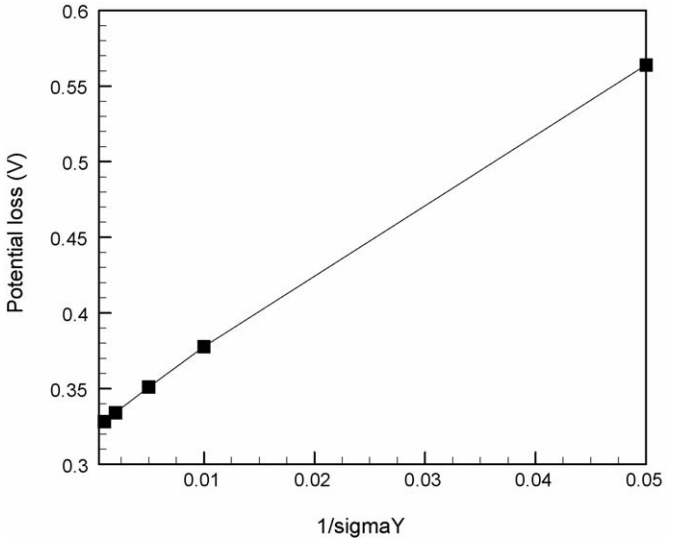

Fig. 8. Potential losses for different GDL electrical conductivities.

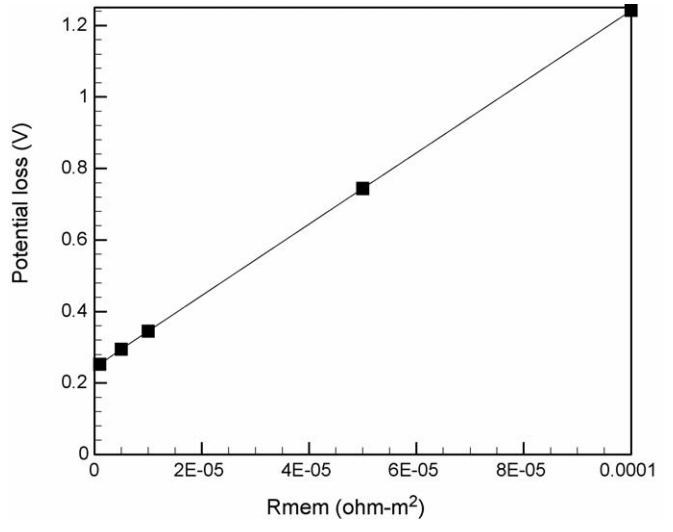

Fig. 10. Potential losses for different membrane conductivities.

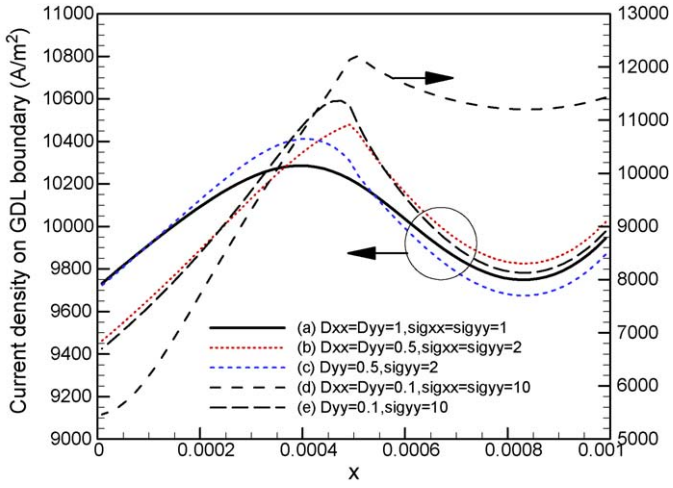

Fig. 11. Current density profiles for different GDL conductivities and diffusivities.

the aforementioned parametric studies, both changes will promote electrical conduction in the GDL and oxygen diffusion will become dominant. Fig. 11 shows the numerical results of current density distribution with properties changed only for the portion of GDL under the land to simulate the effects of compression. The bold line (a) is the baseline case, which uses isotropic properties. When the diffusivity is reduced to half and the conductivity doubled (b) for an isotropic case and (c) for an anisotropic case, departure from the baseline is observed. Further reducing the diffusivity and increasing the conductivity by an order of magnitude (d and e) shows similar trends but more pronounced effects. Fig. 12 compares the oxygen mole fraction distribution and the current flow in the GDL for the baseline case and case (e) in Fig. 11, which has a low through-plane diffusivity (1/10 of the baseline value) and a high through-plane conductivity (10 times of the baseline value) in the under-the-land portion of the GDL. For case (e) the oxygen diffusion into the compressed region is hindered by the low diffusivity, hence the low current density in this region. Due to the relatively high conductivity in the region under the land, most of the current under the channel flows right across the border between the compressed region and the uncompressed region.

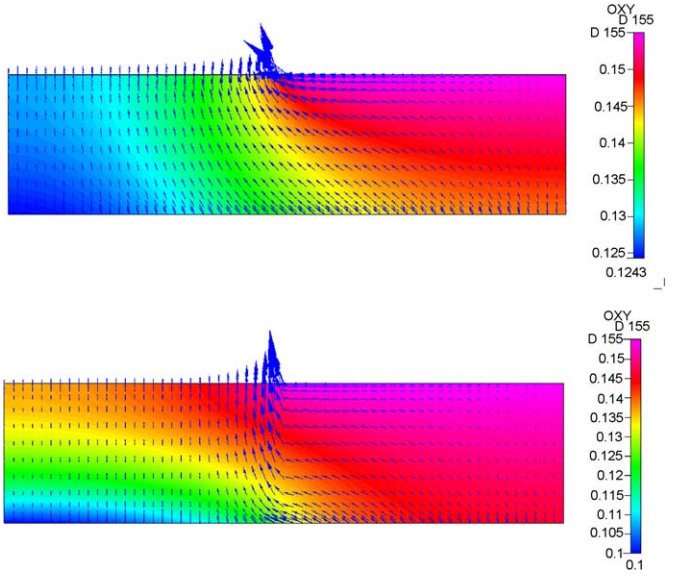

Fig. 12. Oxygen mole fraction in the GDL for different compression conditions (top: baseline, bottom: case (e) in Fig. 11).

3.7. Analysis

Comprehensive 3D CFD-based simulations of the PEMFC have the advantage of providing detailed information of the complex transport phenomena involved in the system. However, using comprehensive CFD simulation tools to gain physical insights and scaling of the problem is computationally expensive. The simplified model of the present study provides a rapid method for analyzing the coupled transport in the MEA. In the present model, the transport of gas species and electron in the GDL are both described by two Laplace equations with similar boundary conditions. The coupling of both transport processes occurs only on one of the domain boundaries, i.e. on the interface of the cathodic catalyst layer and the GDL. The effects of the catalyst layer and the membrane are captured through the potential balance Eq. (5), which essentially is a boundary condition for electrical potential when the entire unit cell (MEA and bipolar plates) is considered. In the model, the potential balance equation is used to evaluate the current density profile on the boundary where coupling of gas species and electron occurs. In fuel cell operation, one is concerned with the distribution of current in the MEA. A current density distribution of minimum spatial variation in general yields an optimal cell performance and implies maximum durability. The gradient of the through-plane current density in the in-plane direction on the catalyst layer–GDL interface can be obtained from the potential balance Eq. (5) by taking the derivative of the potential:

$$\frac{\partial \phi^*}{\partial x} = \frac{\partial \phi_{BC}}{\partial x} + \frac{\partial \eta}{\partial x} + \frac{\partial (iR)}{\partial x} \tag{11}$$

By applying the chain rule to the activation overpotential and the ohmic terms, and with the assumption of a uniform cell potential ϕ^*, we have

$$0 = \frac{\partial \phi_{BC}}{\partial x} + \frac{\partial \eta}{\partial i}\frac{\partial i}{\partial x} + i\frac{\partial R}{\partial x} + R\frac{\partial i}{\partial x} \tag{12}$$

With (6) for the activation overpotential and rearranging (12), we have the gradient of current density as

$$\frac{\partial i}{\partial x} = \frac{-1}{R + \frac{1}{i\alpha_c f}}\left(\frac{\partial \phi_{BC}}{\partial x} + i\frac{\partial R}{\partial x} + \frac{-1}{x_{O_2}\alpha_c f}\frac{\partial x_{O_2}}{\partial x}\right) \tag{13}$$

The three terms in the bracket of (13) represent respectively the contributions due to gradient of electrical conduction in the GDL, variation of protonic resistance in the membrane, and gradient of oxygen distribution in the GDL. Fig. 13 shows the profile of these terms and the profile of predicted current density for the baseline case. One can see that the current density reaches a maximum or minimum at the location where the summation of the three terms in (13) equals zero. The implication of the analysis on the current density gradient is that in order to minimize the gradient of current density in the MEA, one must (a) minimize

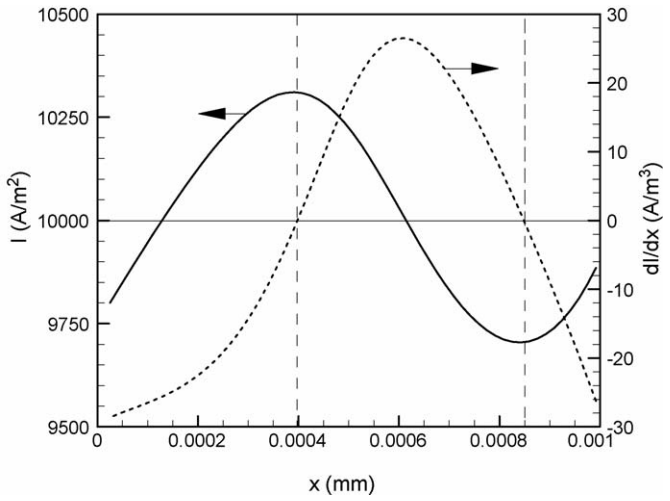

Fig. 13. Profiles of current density and gradient of current density on the interface of the GDL and catalyst layer.

the sum of contributions due to the three major sources of non-uniformity in (13), and (b) increase the membrane resistance, which is undesirable. We note that the first and third terms in the bracket of (13) are of opposite sign under normal conditions. When the land area is wide, or for a GDL material with low in-plane conductivity, the contribution due to electrical conduction in the GDL is relatively small compared to that due to mass diffusion in the GDL. In this case the current gradient is dominated by the oxygen distribution on the catalyst layer surface. On the other hand, for a large channel opening, the effects due to oxygen distribution become less significant and the electrical conduction may become dominant. The balance between the electrical conduction and mass diffusion in the GDL is also affected by the distribution of membrane resistance, which is closely related to current density current density distribution and local humidity.

4. Conclusions

In this work we present a simplified model for simulating coupled electron and mass transport in the GDL of a PEMFC. The parametric study performed using this model shows that current density distribution at the GDL/catalyst interface can be dictated by either electron transport or mass transport in the GDL depending on parameters including channel geometry (land versus channel width), oxygen concentration in the gas channel, transport properties (conductivity and diffusivity), membrane resistance, etc. The model is also capable in predicting the effects due to compression, provided a realistic correlation between compression force and anisotropic transport properties is available. An analysis based on examining the gradients on the catalyst layer surface has shown that the current gradient is dependent on the gradients of electrical potential in the GDL, oxygen concentration and water content in the membrane. The approach presented here provides an effective method for assessing design trade-offs and for optimization of channel dimensions. Ongoing and future work [17] will focus on using this model to provide design guidelines.

Acknowledgements

Funding for this work was provided by the MITACS Network of Centres of Excellence, Ballard Power Systems and the Canada Research Chairs program. The authors wish to also acknowledge insightful inputs from Dr. Brian Wetton.

References

[1] A.A. Kulikovsky, J. Divisek, A.A. Kornyshev, Modeling the cathode compartment of polymer electrolyte fuel cells: dead and active reaction zones, J. Electrochem. Soc. 146 (11) (1999) 3981–3991.
[2] H. Meng, C.Y. Wang, Electron transport in PEFCs, J. Electrochem. Soc. 151 (3) (2004) A358–A367.
[3] P.T. Nguyen, T. Berning, N. Djilali, Computational model of a PEM fuel cell with serpentine gas flow channels, J. Power Sources 130 (1–2) (2004) 149–157.
[4] C. Ziegler, A. Schmitz, M. Tranitz, E. Fontes, J.O. Schumacher, Modeling planar and self-breathing fuel cells for use in electronic devices, J. Electrochem. Soc. 151 (12) (2004) A2028–A2041.
[5] W. Sun, B.A. Peppley, K. Karan, Modeling the influence of GDL and flow-field plate parameters on the reaction distribution in the PEMFC cathode catalyst layer, J. Power Sources 144 (1) (2005) 42–53.
[6] A.Z. Weber, J. Newman, Modeling transport in polymer-electrolyte fuel cells, Chem. Rev. 104 (2004) 4679–4726.
[7] T. Berning, D.M. Lu, N. Djilali, Three-dimensional computational analysis of transport phenomena in a PEM fuel cell, J. Power Sources 106 (2003) 284–294.
[8] S. Mazumder, J.V. Cole, Rigorous 3D mathematical modeling of PEM fuel cells. I. Model predictions without liquid water transport, J. Electrochem. Soc. 150 (11) (2003) A1503–A1509.
[9] W.-K. Lee, S. Shimpalee, J.W. Van Zee, Verifying predictions of water and current distributions in a serpentine flow field polymer electrolyte membrane fuel cell, J. Electrochem. Soc. 150 (2003) A341–A348.
[10] H. Meng, C.Y. Wang, Large-scale simulation of polymer electrolyte fuel cells by parallel computing, Chem. Eng. Sci. 59 (2004) 3331–3343.
[11] Shimpalee, S. Greenway, D. Spuckler, J.W. Van Zee, Predicting water and current distributions in a commercial-size PEMFC, J. Power Sources 135 (2004) 79–87.
[12] B.R. Sivertsen, N. Djilali, CFD based modelling of proton exchange membrane fuel cells, J. Power Sources 141 (2005) 65–78.
[13] K.W. Lum, J.J. McGuirk, Three-dimensional model of a complete polymer electrolyte membrane fuel cell—model formulation, validation and parametric studies, J. Power Sources 143 (1–2) (2005) 103–124.
[14] E. Birgersson, M. Noponen, M. Vynnycky, Analysis of a two-phase non-isothermal model for a PEFC, J. Electrochem. Soc. 152 (5) (2005) A1021–A1034.
[15] W. Sun, B.A. Peppley, K. Karan, An improved two-dimensional agglomerate cathode model to study the influence of catalyst layer structural parameters, Electrochim. Acta 50 (16–17) (2005) 3359–3374.
[16] P.C. Sui, S. Kumar, N. Djilali, Development and validation of advanced computational tools for PEM fuel cell design, in preparation.
[17] P.C. Sui, S. Kumar, N. Djilali, Design and optimization of the gas channels of a PEMFC using CFD-based simulation tools, in: Proceedings of the Fourth Int. ASME Conf. on Fuel Cell Science, Eng. & Technology, Irvine, in press.